

# Magnetic structures and magnetic phase transitions in the Mn-doped orthoferrite $\text{TbFeO}_3$ studied by neutron powder diffraction

Harikrishnan S. Nair,<sup>1, a)</sup> Tapan Chatterji,<sup>2</sup> C. M. N. Kumar,<sup>3, 4</sup> Thomas Hansen,<sup>2</sup>  
Hariharan Nhalil,<sup>5</sup> Suja Elizabeth,<sup>5</sup> and André M. Strydom<sup>1, 6</sup>

<sup>1)</sup> *Highly Correlated Matter Research Group, Physics Department,  
P. O. Box 524, University of Johannesburg, Auckland Park 2006,  
South Africa*

<sup>2)</sup> *Institut Laue-Langevin, BP 156, 38042 Grenoble Cedex 9,  
France*

<sup>3)</sup> *Jülich Centre for Neutron Science JCNS, Outstation at SNS,  
Oak Ridge National Laboratory, Oak Ridge, TN 37831,  
USA*

<sup>4)</sup> *Chemical and Engineering Materials Division, Oak Ridge National Laboratory,  
Oak Ridge, TN 37831, USA*

<sup>5)</sup> *Department of Physics, Indian Institute of Science, Bangalore 560012,  
India*

<sup>6)</sup> *Max Planck Institute for Chemical Physics of Solids (MPICPfs),  
Nöthnitzerstraße 40, 01187 Dresden, Germany*

(Dated: 3 February 2016)

The magnetic structures and the magnetic phase transitions in the Mn-doped orthoferrite  $\text{TbFeO}_3$  studied using neutron powder diffraction are reported. Magnetic phase transitions are identified at  $T_N^{\text{Fe/Mn}} \approx 295$  K where a paramagnetic-to-antiferromagnetic transition occurs in the Fe/Mn sublattice,  $T_{SR}^{\text{Fe/Mn}} \approx 26$  K where a spin-reorientation transition occurs in the Fe/Mn sublattice and  $T_N^R \approx 2$  K where Tb-ordering starts to manifest. At 295 K, the magnetic structure of the Fe/Mn sublattice in  $\text{TbFe}_{0.5}\text{Mn}_{0.5}\text{O}_3$  belongs to the irreducible representation  $\Gamma_4$  ( $G_x A_y F_z$  or  $Pb'n'm$ ). A mixed-domain structure of  $(\Gamma_1 + \Gamma_4)$  is found at 250 K which remains stable down to the spin re-orientation transition at  $T_{SR}^{\text{Fe/Mn}} \approx 26$  K. Below 26 K and above 250 K, the majority phase ( $> 80\%$ ) is that of  $\Gamma_4$ . Below 10 K the high-temperature phase  $\Gamma_4$  remains stable till 2 K. At 2 K, Tb develops a magnetic moment value of  $0.6(2) \mu_B/\text{f.u.}$  and orders long-range in  $F_z$  compatible with the  $\Gamma_4$  representation. Our study confirms the magnetic phase transitions reported already in a single crystal of  $\text{TbFe}_{0.5}\text{Mn}_{0.5}\text{O}_3$  and, in addition, reveals the presence of mixed magnetic domains. The ratio of these magnetic domains as a function of temperature is estimated from Rietveld refinement of neutron diffraction data. Indications of short-range magnetic correlations are present in the low- $Q$  region of the neutron diffraction patterns at  $T < T_{SR}^{\text{Fe/Mn}}$ . These results should motivate further experimental work devoted to measure electric polarization and magnetocapacitance of  $\text{TbFe}_{0.5}\text{Mn}_{0.5}\text{O}_3$ .

Keywords: Orthoferrites, Spin-reorientation, Magnetic structure

---

<sup>a)</sup>Electronic mail: h.nair.kris@gmail.com, hsnair@uj.ac.za

## I. INTRODUCTION

The orthoferrite [ $R\text{FeO}_3$ ;  $R$  = rare earth] oxides have been recently re-investigated experimentally and theoretically from the fascinating perspective of multiferroicity.<sup>1-5</sup> Pursuing the recent line of multiferroics research, theoretical work on  $R\text{FeO}_3$  thinfilms has identified that strain can convert paraelectric phase of orthoferrites in to ferroelectrics thus rendering them multiferroic<sup>5</sup>. It has been found theoretically that for large values of strain on  $R\text{FeO}_3$  with large rare earth ion, giant polarization is realized. In fact, with increasing strain, a new ferroelectric phase, not observed in any perovskite before, is realized. Multifunctional properties like large magnetoelectric coupling and ultrafast optical control of spins have been observed in the orthoferrites<sup>6-8</sup>. The  $R\text{FeO}_3$  realize high Néel temperature,  $T_N \approx 623$  -740 K<sup>9,10</sup> however, in bulk form they are paraelectric rather than ferroelectric suggesting weak multiferroic effects. Weak ferroelectric polarization has been recently reported in Gd and Sm orthoferrites<sup>6,11</sup> which are thought to have "improper" origin induced by magnetic order. In  $\text{TbFeO}_3$ , an unusual incommensurate magnetic phase was discovered through neutron diffraction<sup>12</sup> – it was shown that the exchange of spin waves between extended topological defects could result in novel magnetic phases drawing parallels with the Yukawa forces that mediate between protons and neutrons in a nucleus. The  $\text{Fe}^{3+}$  moments in  $\text{TbFeO}_3$  exhibit  $G_x A_y F_z$  ( $Pb'n'm$ ) spin configuration at room temperature<sup>13-15</sup> which is accompanied by a spin-reorientation to  $F_x C_y G_z$  ( $Pbn'm'$ ). At 3 K, another spin re-orientation occurs to revert to the  $G_x A_y F_z$  ( $Pb'n'm$ ) structure. It is considered that the  $\text{Tb}^{3+}$  spins order in  $F_x C_y$  structure in 10 - 3 K interval and in the  $A_x G_y$  structure below 3 K. Doping the  $R$ -site in  $R\text{FeO}_3$  with another rare earth is found to be profitable to realize electric field induced generation and reversal of ferromagnetic moments<sup>16,17</sup>. Chemical substitution at the Fe-site in  $R\text{FeO}_3$  also brings about interesting multiferroic effects. For example, in the case of Mn-substituted  $\text{YFeO}_3$ , magnetoelectric and magnetodielectric effects at different temperatures were reported<sup>1</sup>. First-order spin-reorientation effects were observed as a result of Mn-substitution however, the magnetodielectric effects were observed at lower temperatures than  $T_N$  or  $T_{SR}$ . Giant magnetodielectric coupling is also observed in another doped-orthoferrite,  $\text{DyMn}_{0.33}\text{Fe}_{0.67}\text{O}_3$ <sup>18</sup>. Spin-reorientation effects and magnetic sublattice effects were also observed in doped-orthoferrites with large  $R$ <sup>19,20</sup>.  $G$ -type magnetic ordering of  $\text{Mn}^{3+}$  and  $\text{Cr}^{3+}$  spins were observed below  $T_N \approx 84$  K in the case of  $\text{TbMn}_{0.5}\text{Cr}_{0.5}\text{O}_3$ <sup>21</sup>, in

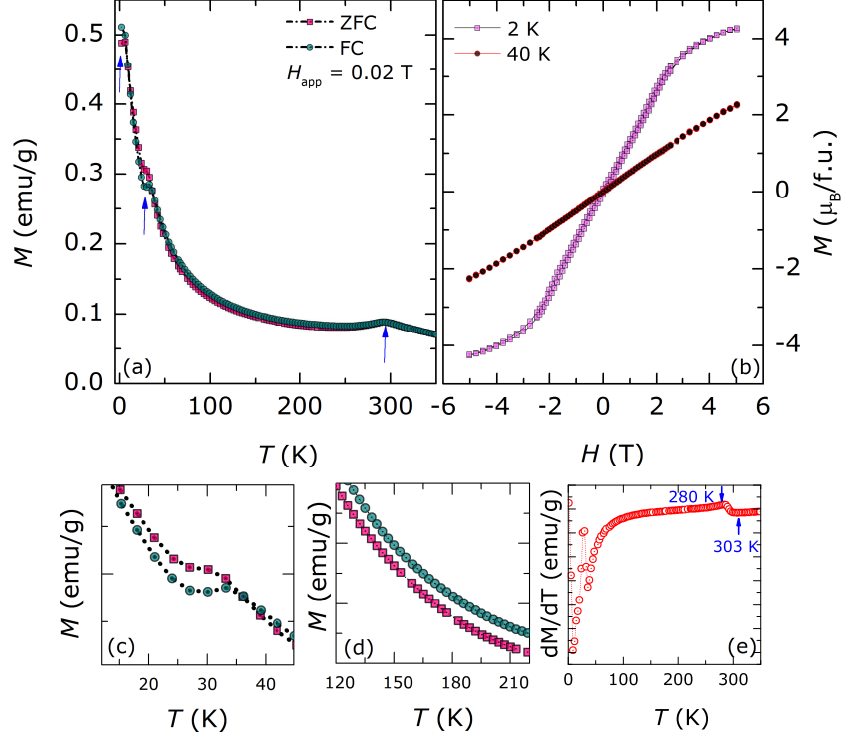


FIG. 1. (color online) (a) The magnetization data of TbFe<sub>0.5</sub>Mn<sub>0.5</sub>O<sub>3</sub> in ZFC and FC protocols at applied field of 0.02 T. Three transitions are visible at  $T_N^{\text{Fe/Mn}} \approx 295$  K,  $T_{SR}^{\text{Fe/Mn}} \approx 26$  K and at  $T_N^{\text{R}} \approx 2$  K. (b) The isothermal magnetization TbFe<sub>0.5</sub>Mn<sub>0.5</sub>O<sub>3</sub> at 2 K and at 40 K. (c) Magnifies the transition at  $T_{SR}^{\text{Fe/Mn}}$  while (d) shows the irreversibility present till  $T_N^{\text{Fe/Mn}}$ . The derivative  $dM/dT$  is shown in (e) to clarify the breadth of the transition at  $T_N^{\text{Fe/Mn}}$ .

addition to signatures of short-range magnetic correlations observed below 40 K which was attributed to the ferromagnetic component from canting of magnetic moments along the *c*-axis. In the case of Mn-substituted compound TbFe<sub>0.75</sub>Mn<sub>0.25</sub>O<sub>3</sub>, the  $T_N$  was determined to be 550 K and the  $T_{SR}$  as 180 K through magnetic studies and Mößbauer spectroscopy<sup>22</sup>.

In our previous investigation using magnetometry it was inferred that TbFe<sub>0.5</sub>Mn<sub>0.5</sub>O<sub>3</sub> orders in  $A_xG_yC_z$  ( $\Gamma_1$ ) structure at  $T_N^{\text{Fe/Mn}} \approx 286$  K followed by a spin re-orientation at  $T_{SR}^{\text{Fe/Mn}} \approx 28$  K to the structure  $G_xA_yF_z$  ( $\Gamma_4$ )<sup>23</sup>. No signature of Tb ordering was obtained in the previous study. In the present manuscript, we make a detailed investigation of the magnetic structures and spin re-orientation transitions in TbFe<sub>0.5</sub>Mn<sub>0.5</sub>O<sub>3</sub> using neutron powder diffraction in order to confirm the magnetic structure arrived at through macroscopic magnetization earlier. We update the magnetic structures as a function of temperature and observe that they evolve between  $\Gamma_1$  and  $\Gamma_4$  through mixed-domains of ( $\Gamma_1 + \Gamma_4$ ).

## II. EXPERIMENTAL DETAILS

Polycrystalline samples of  $\text{TbFe}_{0.5}\text{Mn}_{0.5}\text{O}_3$  were prepared by conventional solid state reaction methods employing the oxides  $\text{Tb}_2\text{O}_3$ ,  $\text{FeO}$ ,  $\text{MnO}_2$  (all from Sigma Aldrich, 99.9%) as precursors. The thoroughly-mixed powder was heated at  $1300^\circ\text{C}$  for 4 days with intermediate grinding. The phase-purity of the black powder that resulted was checked using x ray diffraction employing a Philips X'pert diffractometer with  $\text{Cu-K}\alpha$  radiation. The chemical composition of the prepared sample was determined using the Inductively Coupled Plasma emission Spectroscopy (ICPAES) method. Magnetization measurements were performed on a sintered pellet of the sample in a magnetic property measurement system (MPMS, Quantum Design, San Diego). Neutron powder diffraction experiments were performed on 8 g of  $\text{TbFe}_{0.5}\text{Mn}_{0.5}\text{O}_3$  powder at the instrument D1B in ILL, Grenoble. A wavelength of  $2.52\text{ \AA}$  was used for the experiment. Diffractograms were recorded at 2 K, 5 K, 10 K, 26 K, 50 K to 100 K in 10 K interval and 100 K to 300 K in 50 K interval. The diffraction data was analyzed using FullProf suite of programs<sup>24</sup> employing the Rietveld method<sup>25</sup>. Magnetic structure was determined using the software SARAh<sup>26</sup> and was refined using FullProf.

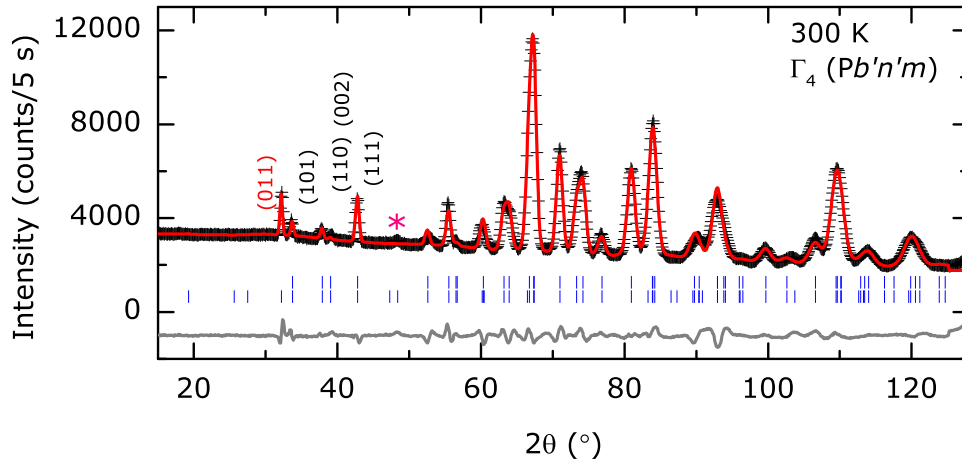


FIG. 2. (color online) The Rietveld refinements of the neutron powder diffraction pattern of  $\text{TbFe}_{0.5}\text{Mn}_{0.5}\text{O}_3$  at 300 K. The nuclear structure is refined using the space group  $Pbnm$ . The magnetic structure conforms to the representation  $\Gamma_4$  or  $G_x A_y F_z$ . The lower set of vertical marks in the figure correspond to the magnetic unitcell and the upper ones to the nuclear. Some of the reflections in the low- $2\theta$  region are shown indexed. An unknown impurity peak is marked with an asterisk.

### III. RESULTS

#### A. Magnetization

The experimentally measured magnetization curves,  $M(T)$ , in zero field-cooled and field-cooled protocols at 0.02 T are plotted in Fig 1 (a) and the isothermal magnetization curves of  $\text{TbFe}_{0.5}\text{Mn}_{0.5}\text{O}_3$  at 2 K and 40 K are presented in (b). Three magnetic phase transitions are identified in (a) *viz.*,  $T_N^{\text{Fe/Mn}} \approx 295$  K,  $T_{SR}^{\text{Fe/Mn}} \approx 26$  K and  $T_N^{\text{R}} \approx 2$  K. The magnetic phase transition at  $T_N^{\text{Fe/Mn}}$  marks the paramagnetic (PM) to antiferromagnetic (AFM) phase transition.  $\text{TbFe}_{0.5}\text{Mn}_{0.5}\text{O}_3$  adopts  $G_x A_y F_z$  magnetic structure below this temperature<sup>23</sup>. The apparent difference seen in the transition temperatures of the single crystal and the polycrystalline sample might stem from differences in sample quality. As determined by the ICPAES method, the chemical composition of the sample is  $\text{Tb}_{1.97}\text{Fe}_{0.51}\text{Mn}_{0.49}\text{O}_3$  which is very close to the nominal value. The second transition occurring at  $T_{SR}^{\text{Fe/Mn}} \approx 26$  K corresponds to the spin-reorientation transition where the structure transforms from  $G_x A_y F_z$  to  $A_x G_y C_z$ . At temperatures close to 2 K, signatures of Tb-order are observed which is reflected in the magnetization measurements at 0.02 T as a irreversibility between the ZFC and FC plots at  $\approx 5$  K. The panel (c) in Fig 1 magnifies the  $M(T)$  curves around  $T_{SR}^{\text{Fe/Mn}}$  where a "loop"-like feature is observed. It can be observed that the "loop"-like feature begins at  $\approx 36$  K and extends till about 18 K. The  $M(T)$  at a higher applied field of 1 T was measured where the signs of magnetic phase transitions or bifurcation between ZFC

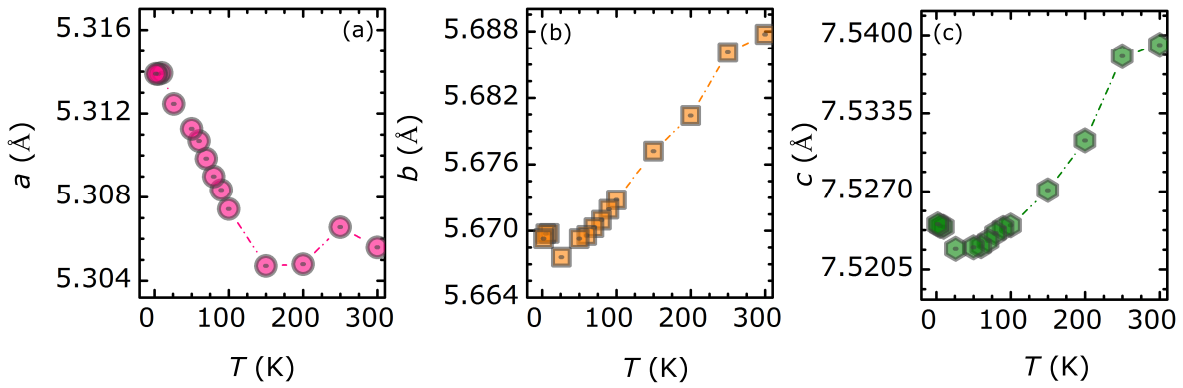


FIG. 3. (color online) The variation of the lattice parameters  $a$ ,  $b$  and  $c$  of  $\text{TbFe}_{0.5}\text{Mn}_{0.5}\text{O}_3$  as a function of temperature.  $b$  and  $c$  follow a similar temperature-dependence while  $a$  shows an increase at low temperature.

and FC were absent (data not shown). The panel (d) shows the presence of irreversibility extends over a wide temperature range from 36 K to  $T_N^{\text{Fe/Mn}}$ . In the panel (e), the derivative  $dM/dT$  versus  $T$  is plotted to show the  $T_N^{\text{Fe/Mn}}$  transition more clearly. It is seen that the  $T_N^{\text{Fe/Mn}}$  is a very broad transition with a spread in temperature from about 280 K extending to 303 K. The transition temperature of 295 K is estimated approximately at the point of steepest slope of  $dM/dT$ .

At 2 K, the maximum magnetization attained with application of 5 T is about  $4 \mu_B/\text{f.u.}$  This value is lower than the value obtained for ferromagnetic alignment of  $\text{Fe}^{3+}$ ,  $\text{Mn}^{3+}$  and  $\text{Tb}^{3+}$  moments. The observed maximum moment at 2 K, 5 T is comparable to the moment value obtained on the single crystal of  $\text{TbFe}_{0.5}\text{Mn}_{0.5}\text{O}_3$  in the case of  $H \parallel b$  at 25 K<sup>23</sup>. The first-order spin-flip-like transition observed at  $H_c \pm 26$  kOe is not clear in the present measurement on polycrystalline sample. Though a weak hysteresis is observed at 2 K in Fig 1 (b), prominent hysteresis loops as observed for  $H \parallel c$  in single crystals are absent.

TABLE I. The refined lattice parameters and fractional coordinates of  $\text{TbFe}_{0.5}\text{Mn}_{0.5}\text{O}_3$  at 300 K, 150 K, 26 K and at 2 K. These parameters are obtained through Rietveld refinement of the neutron powder diffraction data obtained from the instrument D1B, ILL, Grenoble. The nuclear structure model used was  $Pbnm$  with Fe/Mn at  $4b (\frac{1}{2}, 0, 0)$  and Tb at  $4c (x, y, z)$ .

	300 K	150 K	26 K	2 K
$a(\text{\AA})$	5.3055(5)	5.3046(5)	5.3124(4)	5.3138(1)
$b(\text{\AA})$	5.6877(8)	5.6772(6)	5.6676(8)	5.6692(6)
$c(\text{\AA})$	7.5391(9)	7.5270(8)	7.5221(2)	7.5242(4)
Tb: $x$	-0.0173(7)	-0.0193(7)	-0.0223(6)	-0.0202(6)
$y$	0.0715(6)	0.0714(6)	0.0732(5)	0.0712(5)
$z$	0.25	0.25	0.25	0.25
O1: $x$	0.1089(8)	0.1084(9)	0.1091(9)	0.1094(8)
$y$	0.4669(7)	0.4659(8)	0.4665(7)	0.4668(7)
$z$	0.25	0.25	0.25	0.25
O2: $x$	-0.2999(6)	-0.3007(6)	-0.3007(5)	-0.3000(5)
$y$	0.3152(6)	0.3149(5)	0.3145(5)	0.31420(5)
$z$	0.0509(6)	0.0513(6)	0.0549(6)	0.0520(6)

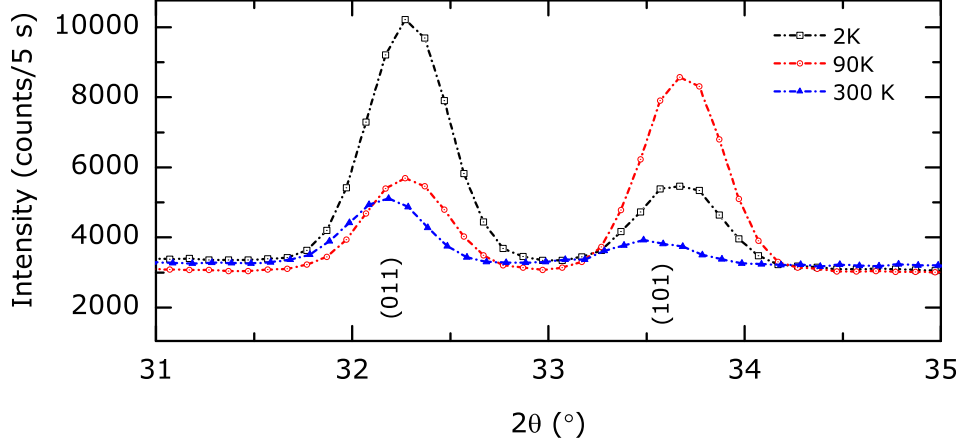


FIG. 4. (color online) Expanded view of the neutron diffraction pattern of  $\text{TbFe}_{0.5}\text{Mn}_{0.5}\text{O}_3$  at 300 K, 90 K and 2 K that shows the evolution of intensity of the (011) and the (101) reflections.  $I_{(011)} > I_{(101)}$  is observed at 2 K while at 90 K, the opposite is true. At 300 K, again the condition  $I_{(011)} > I_{(101)}$  is satisfied.

These features underline the magnetic anisotropy in the crystal sample of  $\text{TbFe}_{0.5}\text{Mn}_{0.5}\text{O}_3$ <sup>23</sup>.

## B. Neutron diffraction

The neutron diffraction patterns at different temperature points were refined using FullProf. The values of refined lattice parameters and fractional atomic coordinates of  $\text{TbFe}_{0.5}\text{Mn}_{0.5}\text{O}_3$  at 300 K, 150 K, 26 K and 2 K are collected in Table I. The temperature-dependent variation of the lattice parameters  $a$ ,  $b$  and  $c$  are shown in Fig 3. No significant anomalies are observed for the unit cell parameters as a function of temperature except for a change-of-slope at 150 K and 250 K. However, lack of enough data points makes any inference unreliable here. The trend of thermal evolution of  $b$  and  $c$  are comparable while that of  $a$  is opposite to the other two. Jahn-Teller (JT) or pseudo-JT distortion has been correlated with the observation of multiferroicity in perovskites<sup>27</sup> including  $\text{TbMnO}_3$  which are known to show significant JT effect<sup>28</sup>. In order to investigate the presence of JT effect in  $\text{TbFe}_{0.5}\text{Mn}_{0.5}\text{O}_3$ , estimates of the distortion parameters and bond angles and bond distances were obtained from the refined structural data, Table II. However, with the substitution of 50% Fe at the Mn-site, the effects of JT-distortion are found to have diminished in  $\text{TbFe}_{0.5}\text{Mn}_{0.5}\text{O}_3$  however, effects of distortion of the perovskite structure are clearly seen.

TABLE II. The bond distances and bond angles of  $\text{TbFe}_{0.5}\text{Mn}_{0.5}\text{O}_3$  at 300 K, 150 K, 26 K and at 2 K. These parameters are obtained through Rietveld refinement of the neutron powder diffraction data at the respective temperatures. The Jahn-Teller parameters are tabulated for different temperatures. For a comparison, the JT-values for  $\text{TbMnO}_3$  at 300 K collected from Ref.[28] and given in parenthesis.

	300 K	150 K	26 K	2 K
Mn–O(2)	$l=2.123(4) \times 2$ $s=1.947(6) \times 2$	$l=2.112(5) \times 2$ $s=1.949(6) \times 2$	$l=2.114(6) \times 2$ $s=1.956(7) \times 2$	$l=2.111(5) \times 2$ $s=1.951(7) \times 2$
Mn–O(1)	$m=1.977(8) \times 2$	$m=1.977(7) \times 2$	$m=1.977(8) \times 2$	$m=1.978(6) \times 2$
Mn–O(2)–Mn	145.81(8)	146.06(9)	145.14(7)	145.81(11)
Mn–O(1)–Mn	144.9(12)	144.2(10)	144.04(8)	144.9(9)
O(1)–Mn–O(1)	180	180	180	180
O(2)–Mn–O(2)	$90.57(12) \times 2$ $89.53(9) \times 2$	$90.60(8) \times 2$ $89.40(6) \times 2$	$90.16(11) \times 2$ $89.83(9) \times 2$	$90.41(8) \times 2$ $89.59(7) \times 2$
$Q_2 = 2(l - s)/\sqrt{2}$	0.2489 (0.45)	0.2305	0.2234	0.2263
$Q_3 = 2(2m - l - s)/\sqrt{6}$	-0.0947 (-0.2)	-0.0874	-0.0947	-0.0865
$\phi = \tan(Q_3/Q_2)$	-20.84° (-24)	-20.77°	-22.98°	-20.92°
$\rho_0 = \sqrt{Q_3^2 + Q_2^2}$	0.266 (0.5)	0.2465	0.2426	0.2423

To facilitate comparison, in Table II, the values of the JT-parameters of  $\text{TbMnO}_3$  at 300 K taken from Ref.[28]<sup>28</sup> are given in parenthesis.

A symmetry analysis of  $R\text{FeO}_3$  in  $Pbnm$  space group with  $\text{Fe}^{3+}$  in  $4b$  and  $R^{3+}$  in  $4c$  Wyckoff positions leads to eight irreducible representations,  $\Gamma_1$  through  $\Gamma_8$ , for magnetic structure. For the  $4b$  position, the configurations  $\Gamma_5$  to  $\Gamma_8$  are not allowed and hence  $\Gamma_1$ ,  $\Gamma_2$ ,  $\Gamma_3$  and  $\Gamma_4$  are selected as the final possibilities. Table III lists these irreducible representations, the Shubnikov space groups and the magnetic structure notations used for  $R\text{FeO}_3$  in general. The neutron diffraction pattern of  $\text{TbFe}_{0.5}\text{Mn}_{0.5}\text{O}_3$  at 300 K is presented in Fig 2 as black plus signs. The nuclear structure at 300 K is refined in  $Pbnm$  space group. In Fig 2, the calculated pattern is shown as red solid line, difference curve as gray dotted line and the allowed Bragg peaks for  $Pbnm$  space group as vertical bars. From the magnetization measurements presented in Fig 1 (a, e), it is clear that  $\text{TbFe}_{0.5}\text{Mn}_{0.5}\text{O}_3$

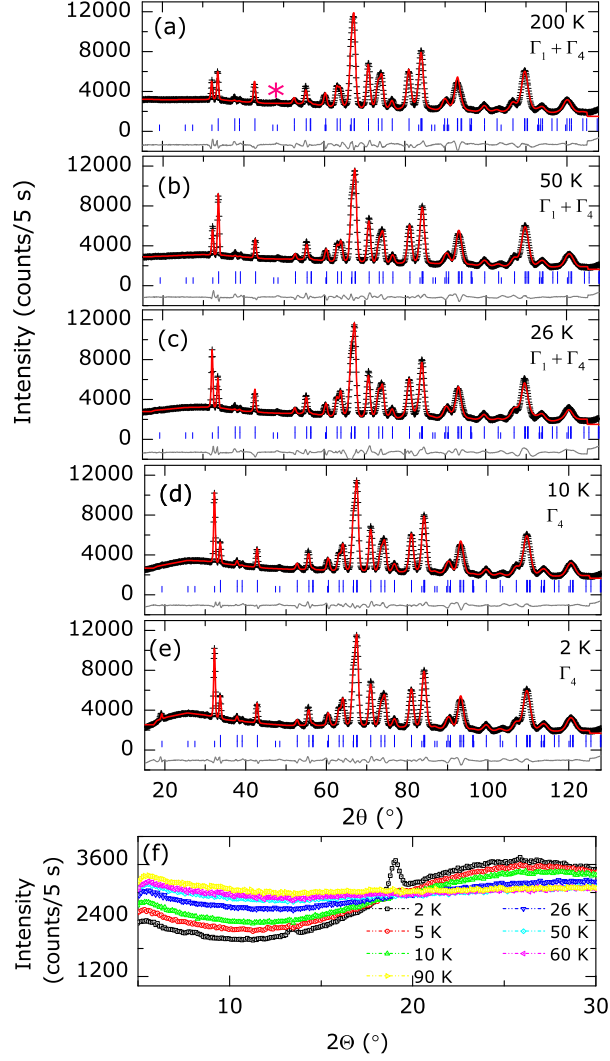


FIG. 5. (color online) The Rietveld refinements of the neutron diffraction pattern of  $\text{TbFe}_{0.5}\text{Mn}_{0.5}\text{O}_3$  at (a) 200 K, (b) 50 K, (c) 26 K and (d) 10 K (e) 2 K. The different magnetic structures at each temperature is indicated in each panel. Recall that at 300 K (Fig. 2)  $\Gamma_4$  prevails as a single phase. The unknown peak at  $\approx 48^\circ$  is marked using an asterisk in (a). (f) Shows the presence of strong diffuse scattering in the low-angle region at  $T < T_{SR}^{\text{Fe/Mn}}$ . Such a diffuse feature is related to the spin fluctuations in the Tb-sublattice.

undergoes a magnetic phase transition very close to 300 K (notice from Fig 1 (e) that the transition extends over a wide range from 280 K to 303 K). Hence, the diffraction data at 300 K is refined with additional magnetic phase. In order to solve the magnetic structure at 300 K, the peaks below  $2\theta \approx 40^\circ$  were used to perform a  $\mathbf{k}$ -search to find the propagation vector. The utility called  $\mathbf{k}$ -search within FullProf suite of programs was used for this

purpose. Thus,  $\mathbf{k}=(000)$  was identified as the propagation vector. Representation analysis using  $\mathbf{k}(000)$  and  $Pbnm$  nuclear cell lead to the listing of four possibilities –  $\Gamma_1$  ( $Pbnm$ ),  $\Gamma_2$  ( $Pbn'm'$ ),  $\Gamma_3$  ( $Pb'nm'$ ) and  $\Gamma_4$  ( $Pb'n'm$ ) matching with the selection in Table III. They also match with the magnetic structures of orthoferrites already reported in the literature<sup>3</sup>. From the refinement trials it was noted that the representation  $\Gamma_3$  contributes zero intensity to the Bragg peaks at (101) and (011) and hence can be excluded. A better visual fit to the experimental data and reasonable agreement factors were obtained for  $\Gamma_4$  (the  $R_{\text{mag}}$  factors were,  $\Gamma_1 \approx 70$ ;  $\Gamma_2 \approx 21$ ;  $\Gamma_3 \approx 20$  and  $\Gamma_4 \approx 5$ ) and hence was accepted as the solution to the magnetic structure at 300 K. In Fig 2, the lower set of vertical tick marks correspond to the magnetic Bragg positions.

After confirming the room-temperature crystal structure to be  $Pbnm$  and the magnetic structure as  $\Gamma_4$  ( $Pb'n'm$ ), we now discuss the low temperature diffraction data. In Fig 4, an expanded view of the reflections in the  $2\Theta$ -range  $31\text{--}35^\circ$  is given for 2 K, 90 K and 300 K. At 2 K, the intensity of the (011) reflection is observed to increase, compared to the value at 300 K. The relative intensity,  $I_{(011)}/I_{(101)} > 1$  at 2 K and 300 K where as the opposite is true for 90 K. Macroscopic magnetic characterization of  $\text{TbFe}_{0.5}\text{Mn}_{0.5}\text{O}_3$ <sup>23</sup> clearly suggested spin-reorientations and magnetic phase transformations as a function of temperature and magnetic fields. At 250 K, the nuclear structure was refined in  $Pbnm$  and the magnetic structure in  $\Gamma_4$  ( $Pb'n'm$ ) similar to the case of 300 K-data. However, at 200 K mixed magnetic domains consisting of  $(\Gamma_1 + \Gamma_4)$  is found to reproduce the experimental data faithfully. Neither of the representations  $\Gamma_1$  or  $\Gamma_4$  alone could give a satisfactory fit, while the mixed-domain model significantly returned lower values of reliability factors ( $R \sim$

TABLE III. The possible magnetic structures of  $R\text{FeO}_3$  allowed by symmetry. The space group is chosen as  $Pbnm$  and  $x$ ,  $y$  and  $z$  denote orientations parallel to the crystallographic directions  $a$ ,  $b$  and  $c$ .  $R$  occupies  $4c$  and Fe,  $4b$  Wyckoff positions in this structure.

Irreps	Space group	$4b$	$4c$
$\Gamma_1$	$Pbnm$	$A_x G_y C_z$	$C_z$
$\Gamma_2$	$Pbn'm'$	$F_x C_y G_z$	$F_x C_y$
$\Gamma_3$	$Pb'nm'$	$C_x F_y A_z$	$C_x F_y$
$\Gamma_4$	$Pb'n'm$	$G_x A_y F_z$	$F_z$

5.3 for mixed-domains whereas  $\sim 6$  for pure phases). A better fit using the mixed-domain model could result from utilizing a bigger parameter space for least-squares however, we also notice the presence of clear irreversibility in the magnetization profiles that are in support of the claim of presence of mixed-domains. The mixed-domains of  $(\Gamma_1 + \Gamma_4)$  were found to exist down till  $T_{SR}^{\text{Fe/Mn}}$  at 26 K. Fig 1 shows that "loop-like" anomalies are present in the  $M(T)$  which correspond to the spin-reorientation transition at  $T_{SR}^{\text{Fe/Mn}}$ . In fact, from the panel (c) of Fig 1 it can be seen that the irreversibility in ZFC and FC curves commences at 36 K itself. Finally at 10 K, the  $\Gamma_4$  representation observed at 300 K re-emerges. It was observed that the inclusion of Tb moments in the refinement at 10 K and 5 K did not lead to any appreciable values of refined magnetic moment on the Tb site. At 2 K, the magnetic structure remains in the  $\Gamma_4$  representation however, Tb develops a magnetic moment value of 0.6(2)  $\mu_B/\text{f.u.}$  indicating that Tb is magnetically ordered at this temperature. The irreversibility in  $M(T)$  suggesting magnetic ordering in the rare earth sublattice occurs  $\approx 5$  K. However, attempts to refine the 5 K-data assuming magnetic contribution from Tb did not yield better agreement factors. Hence magnetic contributions from Mn/Fe were only considered. The refinement of the magnetic structure of Tb was performed in  $F_z$  representation following the symmetry analysis<sup>3</sup>. In Fig 5 (a)–(e), the refined diffraction patterns of  $\text{TbFe}_{0.5}\text{Mn}_{0.5}\text{O}_3$  at 200, 50, 26, 10 K and 2 K are shown. Though no structural distortions are observed in the entire temperature range of the study, the magnetic structure is seen to evolve between the  $\Gamma_4$  and  $\Gamma_1$  representation through mixed-domain regions. A schematic of the magnetic structures  $\Gamma_1$  and  $\Gamma_4$  are shown in Fig 6. In the case of  $\Gamma_4$ , the  $F_z$  type ordering of Tb ions are also depicted (Tb moments are shown in blue). Next, we make an attempt to quantify the volume fraction of the two magnetic domains  $\Gamma_1$  and  $\Gamma_4$ . For this calculation we assume that the total Fe/Mn ordered moment at a particular temperature is equal for both  $\Gamma_1$  and  $\Gamma_4$  domains. With this assumption and by setting the scale factors of both  $\Gamma_1$  and  $\Gamma_4$  domains equal to that of the nuclear phase, the ratio of refined ordered moments of  $\Gamma_1$  and  $\Gamma_4$  should give the percentage of each domains. The result of this calculation is presented as Fig 7. As clear from the figure, mixed domain structure is present in the wide temperature range of 250 K to 26 K. Outside this temperature window, the major magnetic phase is that of  $\Gamma_4$ .

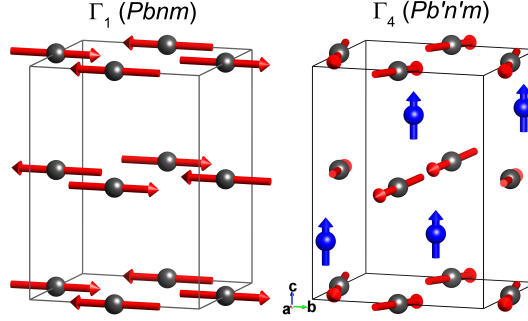


FIG. 6. (color online) The (left)  $\Gamma_1$  and (right)  $\Gamma_4$  magnetic structures of  $\text{TbFe}_{0.5}\text{Mn}_{0.5}\text{O}_3$ . For the  $\Gamma_4$  structure, the Tb magnetic moments are also presented (in blue). The magnitude of Tb moments have been scaled  $\times 2$  for the sake of clarity in viewing.

#### IV. DISCUSSION

Our investigation of the magnetic structure of  $\text{TbFe}_{0.5}\text{Mn}_{0.5}\text{O}_3$  shows that the predominant structures are  $\Gamma_4$  and  $\Gamma_1$  however, a competition between these two magnetic phases is evident from the presence of a mixed-domains in certain temperature range. At 295 K, the high temperature paramagnetic phase transforms to the magnetic structure  $\Gamma_4$  ( $G_x A_y F_z$  or  $Pb'n'm$ ). It is seen that down till  $\approx 250$  K, the  $\Gamma_4$  structure remains stable. In the intermediate temperature range close to 200 K a mixed-domains of ( $\Gamma_1 + \Gamma_4$ ) is observed which remains down till 26 K. A precise phase space study to determine the boundaries of the mixed phase would demand many more temperature points, but such a detailed study was outside the design and scope of our present experiments. As evidenced by the  $M(T)$  curve (Fig 1 (a)), the  $T_{SR}^{\text{Fe/Mn}}$  is associated with a clear bifurcation of ZFC and FC forming a "loop-like" region between 18 K and 36 K. We deduce that the mixed-domains extend over this temperature window. Further at 10 K, the  $\Gamma_4$  structure reemerges and remains till 2 K. In the temperature range 2 - 10 K, the magnetic representation  $\Gamma_1$  leads to a high  $R_{\text{mag}} \approx 60$ . It did not adequately account for the magnetic peaks and hence,  $\Gamma_4$  ( $R_{\text{mag}} \approx 3.5$ ) was chosen as the solution. Note that in both  $\Gamma_1$  and  $\Gamma_4$ , Fe/Mn are constrained to have magnetic moments in  $x$ ,  $y$  and  $z$  whereas the  $R$ -moment is constrained to the  $z$ -direction. We found that in whole temperature range in  $\Gamma_1$  setting the Fe/Mn magnetic moments had negligible  $x$  and  $z$  components (practically zero) and aligned along  $y$ -axis (Fig. 6). Also the whole temperature range in  $\Gamma_4$  setting Fe/Mn moments have negligible  $y$ -component and

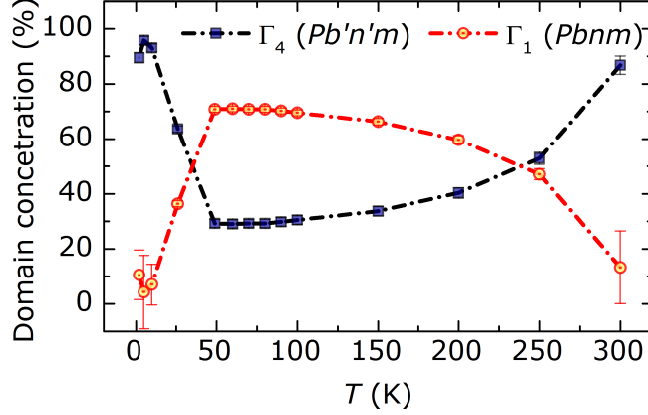


FIG. 7. (color online) The volume fraction of the different magnetic domains  $\Gamma_1$  and  $\Gamma_4$  plotted as a function of temperature. Between 26 K and 250 K the co-existence of both the domain fractions lead to the irreversibility seen in magnetization measurements.

aligned along  $x$ -axis with small canting along  $y$ -direction.

Different rare earths in  $R\text{FeO}_3$  are observed to have different magnetic structures at low temperatures. For example,  $\text{DyFeO}_3$  has a  $Pb'n'm'$  space group for Dy and  $Pnma$  for Fe whereas  $\text{TbFeO}_3$  has  $Pbnm'$  for Tb. In the present case of  $\text{TbFe}_{0.5}\text{Mn}_{0.5}\text{O}_3$ , it is found that in the low temperature region significant diffuse scattered intensity is present arising from the short-range magnetic order of Tb. Supporting this feature is the fact that no enhancement on quality of the fit was obtained in refining the 5 K or 10 K diffraction data by introducing a magnetic moment for Tb. Only at 2 K does Tb begin to order as  $F_z$  as evident by the development of  $0.6(2) \mu_B$  for Tb moment. A notable difference of the magnetic structure of Fe/Mn in  $\text{TbFe}_{0.5}\text{Mn}_{0.5}\text{O}_3$  compared to that of the parent compound  $\text{TbFeO}_3$  is that the latter compound transforms to  $\Gamma_2$  ( $F_x C_y G_z$ ) structure at the spin-reorientation transition. In both the cases, the high temperature structure pertaining to Fe/Mn is  $\Gamma_4$ . In  $\text{TbFeO}_3$ , the Tb moment undergoes two types of ordering below 10 K in to  $F_x C_y$  and to  $A_x G_y$  whereas in  $\text{TbFe}_{0.5}\text{Mn}_{0.5}\text{O}_3$ , Tb develops no significant magnetic moment until 2 K where it orders  $F_z$ .

## V. CONCLUSIONS

In conclusion, the Mn-doped orthoferrite compound  $\text{TbFe}_{0.5}\text{Mn}_{0.5}\text{O}_3$  orders antiferromagnetically at  $T_N^{\text{Fe/Mn}} \approx 300$  K and undergoes spin-reorientation transition at  $T_{SR}^{\text{Fe/Mn}} 26$  K.

Further, at 2 K the rare earth Tb is found to be magnetically ordered, however, the exact ordering temperature is not confirmed through our study. It is found that in the intermediate temperatures 250 K to 26 K, a mixed-domain model best describes the neutron diffraction data. At 2 K and at 300 K  $\Gamma_4$  representation is stable while at the spin-reorientation transition and around 200 K mixed-domains of  $(\Gamma_1 + \Gamma_4)$  exist. An estimate of the domain concentration as a function of temperature is made. Clear indication of diffuse magnetic scattering from Tb is present especially below the  $T_{SR}^{\text{Fe/Mn}}$  while long-range order emerges at 2 K.

## ACKNOWLEDGEMENTS

H. S. N. acknowledges FRC/URC of UJ for a postdoctoral fellowship. A. M. S. thanks the SA-NRF (93549) and the FRC/URC of UJ for financial assistance.

## REFERENCES

- <sup>1</sup>P. Mandal, V. S. Bhadram, Y. Sundarayya, C. Narayana, A. Sundaresan, and C. N. R. Rao, Phys. Rev. Lett. **107**, 137202 (2011).
- <sup>2</sup>M. Shang, C. Zhang, T. Zhang, L. Yuan, L. Ge, H. Yuan, and S. Feng, Appl. Phys. Lett. **102**, 062903 (2013).
- <sup>3</sup>G. Deng, P. Guo, W. Ren, S. Cao, H. E. Maynard-Casely, M. Avdeev, and G. J. McIntyre, J. Appl. Phys. **117**, 164105 (2015).
- <sup>4</sup>V. V. Pavlov, A. R. Akbashev, A. M. Kalashnikova, V. A. Rusakov, A. R. Kaul, M. Bayer, and R. V. Pisarev, J. Appl. Phys. **111**, 056105 (2012).
- <sup>5</sup>H. J. Zhao, Y. Yang, W. Ren, A. Mao, X. M. Chen, and L. Bellaiche, J. Phys.: Condens. Matter **26**, 472201 (2014).
- <sup>6</sup>Y. Tokunaga, S. Iguchi, T. Arima, and Y. Tokura, Phys. Rev. Lett. **101**, 097205 (2008).
- <sup>7</sup>K. Yamaguchi, T. Kurihara, Y. Minami, M. Nakajima, and T. Suemoto, Phys. Rev. Lett. **110**, 137204 (2013).
- <sup>8</sup>R. V. Mikhaylovskiy, E. Hendry, V. V. Kruglyak, R. V. Pisarev, T. Rasing, and A. V. Kimel, Phys. Rev. B **90**, 184405 (2014).
- <sup>9</sup>M. Marezio, J. P. Remeika, and P. D. Dernier, Acta Crystallogr. B **26**, 2008 (1970).

- <sup>10</sup>M. Eibschütz, S. Shtrikman, and D. Treves, Phys. Rev. **156**, 562 (1967).
- <sup>11</sup>J. H. Lee, Y. K. Jeong, J. H. Park, M. Oak, H. M. Jang, J. Y. Son, and J. F. Scott, Phys. Rev. Lett. **107**, 117201 (2011).
- <sup>12</sup>S. Artyukhin, M. Mostovoy, N. P. Jensen, D. Le, K. Prokes, V. G. de Paula, H. N. Bordallo, A. Maljuk, S. Landsgesell, H. Ryll, *et al.*, Nature Mater. **11**, 694 (2012).
- <sup>13</sup>J. E. Bouree and J. Hammann, J. Phys. **36**, 391 (1975).
- <sup>14</sup>E. F. Bertaut, J. Chappert, J. Mareschal, J. P. Rebouillat, and J. Sivardiere, Solid State Commun. **5**, 293 (1967).
- <sup>15</sup>J. Tejada, X. X. Zhang, A. Roig, O. Nikolov, and E. Molins, Europhys. Lett. **30**, 227 (1995).
- <sup>16</sup>Y. Tokunaga, Y. Taguchi, T. Arima, and Y. Tokura, Nature Physics **8**, 838 (2012).
- <sup>17</sup>Y. Tokunaga, Y. Taguchi, T. Arima, and Y. Tokura, Phys. Rev. Lett. **112**, 037203 (2014).
- <sup>18</sup>F. Hong, Z. Cheng, and X. Wang, J. Appl. Phys. **112**, 013920 (2012).
- <sup>19</sup>Y. Nagata, S. Yashiro, T. Mitsuhashi, A. Koriyama, Y. Kawashima, and H. Samata, J. Magn. Magn. Mater. **237**, 250 (2001).
- <sup>20</sup>M. Mihalik, M. Mihalik, M. Fitta, M. Bałanda, M. Vavra, S. Gabáni, M. Zentková, and J. Briančin, J. Magn. Magn. Mater. **345**, 125 (2013).
- <sup>21</sup>M. Staruch, V. Sharma, C. dela Cruz, R. Ramprasad, and M. Jain, J. Appl. Phys. **116**, 033919 (2014).
- <sup>22</sup>W. Kim, B. Y. Kum, and C. S. Kim, J. Supercond. Novel Magn. **24**, 867 (2011).
- <sup>23</sup>N. Hariharan, H. S. Nair, S. Kumar, A. M. Strydom, and S. Elizabeth, J. Appl. Phys. **117**, 173904 (2015).
- <sup>24</sup>J. Rodriguez-Carvajal, LLB, CEA-CNRS, France [<http://www.ill.eu/sites/fullprof/>] (2010).
- <sup>25</sup>H. M. Rietveld, J. Appl. Cryst. **2**, 65 (1969).
- <sup>26</sup>A. S. Wills, Physica B **276**, 680 (2000).
- <sup>27</sup>I. B. Bersuker, Phys. Rev. Lett. **108**, 137202 (2012).
- <sup>28</sup>S. Zhou, L. Shi, H. Yang, and J. Zhao, Appl. Phys. Lett. **91**, 172505 (2007).